Impact of External Forces on the quality of Digital Elevation Model Derived from Drone Technology

Isola, A.,[1*] Mansor, S.,[2] Shafri, H. M.,[3] Pradhan, B.[4] and Mansor, Y.[5]
Geospatial Information Science Research Centre (GISRC), Faculty of Engineering, Universiti Putra Malaysia, 43400 UPM Serdang, Malaysia, E-mail: ajibolaisola3@gmail.com,[1] shattri@gmail.com,[2] hms04@gmail.com,[3] biswajeet24@gmail.com,[4] yaakobms@gmail.com[5]
**Correspondence author*

Abstract
Platform instability is one of the sources of error of Digital Elevation Model (DEM) derived from a low altitude aircraft. This paper examines the influence of atmospheric pressure (AP) on the DEM produced by drone system. To achieve the research objective, an experimental-based fixed-wing drone platform was set up at the Universiti Putra Malaysia Campus. First, Ground Control Points (GCPs) and Check Points (CPs) were established within the study area by a real-time kinematic differential global positioning system. The drone flew seven times at different altitudes over the study area. In the process, an on-board canon digital camera took a series of overlapping photos. The photos were processed with an image-matching algorithm. Then orthorectified the photos using the GCPs. Photo orthorectification entails orientation of aerial photos with respect to the ground control points. It helps to remove distortions that might occur while acquiring or processing the aerial photographs. In the end, seven DEMs were exported in tiff file format. Analysis of impact of AP on the resulting DEMs was conducted using a proposed model and obtained 0.072m, 0.05m, 0.014m, 0.01m, 0.004m, 0.003m, and 0.002m for 100m, 150m, 200m, 250m, 350m, 400m, and 500m altitudes, respectively. To confirm the efficiency of the proposed model, the results were tested using the CPs and their corresponding points on the DEMs and obtained root mean square error of 0.03m, 0.05m, 0.07m, 0.1m, 0.13m, 0.14m, and 0.16m. On a final note, a close look at the validation and impact of AP results unveils a small gap. Hence, suggests that platform instability should be ignored amidst of other external forces that can influence the performance of drone system.

1. Introduction

Accurate Digital Elevation Model (DEM) is a norm for precise applications. DEM can be produced using different techniques (Forkuor and Maathuis, 2012). Satellite and aircraft are mostly used for large and difficult terrain (Thomas et al., 2014). One of the benefits of satellite platform over aircraft is the limitless access to data without being restricted by the government. However, data collected from satellite sensors are mostly affected by cloud and are not suitable for low relief areas (Mercuri et al., 2006). A new trend in the satellite system is GeoEye-1. Although, GeoEye-1 can produce images with a ground resolution of 0.46m in the panchromatic mode and 1.84m in the multi-spectral mode (Cheng and Chaapel, 2014 and Aguilar et al., 2011). Yet, this satellite mapping platform is costly for small areas. Hence, ignite the use of Unmanned Aerial Vehicles system (UAVs) for 3D mapping.

UAV or drone is a pilotless aircraft in which its aircrew has been removed and replaced by a computer system and a radio link (Austin, 2010). UAV remote sensing mapping has potential to provide detailed information about small, accessible, and inaccessible areas in a cost effective manner. However, it is not suitable for mapping vegetated terrain due to the tree's foliage that might block sensors from taken photos. Besides, rules and regulations introduced by many countries are another bottleneck of UAV system (Nex, 2016). UAV has become a necessary tool for both military and civilian operations. The use of UAVs for civilian applications began early 1980s due to the recent advances in imaging sensors and platform miniaturization (Ajibola and Mansor, 2013). Since then UAVs have been widely used as a tool for solving environmental problems (Akbari et al., 2016, Ajibola et al., 2015, Khairul and Anuar, 2013, Wechsler, 2006, Walker and Willgoose, 1999 and Moore et al., 1991). The quality of DEM produced by drone system like other techniques can be influenced with both external and internal forces; even with advances in sensor, processing skills, and

miniaturization of drone platforms (Komarek et al., 2016 and Papasaika-Hanusch, 2012).

Internal sources of error can be caused by the failure of inbuilt system components of an aircraft (Li et al., 2015). Previous studies have shown the effect of internal factors on the quality and performance of aerial vehicles. Prominent among them is the use of equations of motion developed by (Boschetti et al., 2010). External factors, such as atmospheric pressure (AP) and other gases are types of aerodynamic forces. Error in UAV DEM can be caused by the failure of aircraft components and by external forces acting on the aircraft fuselage. Thus, this study aimed to study the effect of AP on the quality of DEM produced by the UAV system.

2. Materials and Method

2.1 Aircraft Stability and Control

This section focuses on the stability and control of a rigid body (e.g. manned and unmanned aircraft). Stability and control affect aircraft's response to perturbations (Boschetti et al., 2010). Aircraft's performance and quality are two different phenomena. The latter is based on the concept that an aircraft is a point with its mass concentrated in its centre of gravity. While the former defined an aircraft as a three-dimensional object, in which its speed is directly related to the three axes of rotation. Hence, the theory of stability and control of a rigid body (Hull, 2007 and Edwards, 1988).

In physics, a rigid body is a body assumed not to be disturbed under the influence of external forces. This is never exist according to the theory of special relativity. The two types of external forces are body forces and surrounding forces. Body forces occur on aircraft from a distance within the aircraft's fuselage, while the surrounding forces are as a result of contact between aircraft and pressure (Talay, 1975). Figure 1 shows the different types of aerodynamics forces that can act on an aircraft. The forces (weight, lift, thrust, drag and skin friction) are caused by the flow of air over the surface of the aircraft (Marzocca, 2013). In the design stage, the weight of an aircraft is always considered to ensure flight stability. The unsteady aerodynamic forces play primary roles in aircraft response to perturbations (AGARD, 1980). Lift is the force opposing the weight and at the same time can prevent an aircraft from falling. In order for an aircraft to take off, force equal or more than its weight must be exerted by an aerofoil and its thrust must exceed the drag. Likewise, thrust is the force opposes drag. It is generated through the propulsion of an engine. Drag is aerodynamic force that acts on all things in motion and should be overcome.

To control an aircraft requires orientation and position relative to its body axis (Marzocca, 2013). Aircraft can be controlled by means of three critical flight dynamics parameters, such as pitch, roll and yaw showed in Figure 1, which are invented by the Wright brothers in 1903 (Kalra et al., 2014, Padfield and Lawrence 2003 and Sciavicco and Siciliano, 2000). Since then, both manned and unmanned aircraft have been designed to navigate in three-dimensional space. Actuators control axes of rotation, which intersected at the centre of gravity of an aircraft. The control is done, such that the pitch (Y-axis) controls aircraft to nose up or down. Roll angle (X-axis) moves the wings right or left and the yaw (Z-axis) controls the nose side to side.

2.2 Relationships between Altitude and Atmospheric Pressure

In this section, analysis of external forces acting on a fixed-wing UAV is carried out by considering the relationships between altitude and AP. In essence, the amount of air molecules in the space decreases as altitude increases and conversely (Paul and Ferl, 2006). Thus, aircraft collecting data at a low altitude will encounter a large amount of AP than it does by a high altitude aircraft. This line of thought is proved by the Bernoulli's theorem of equation of continuity (Ehernberger, 1992).

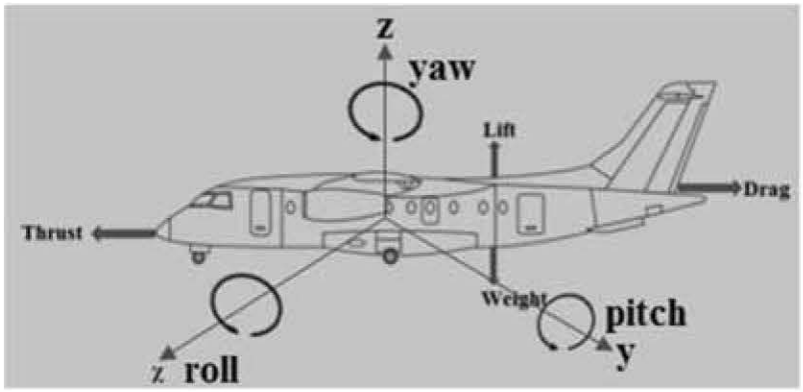

Figure 1: Aircrafts aerodynamics forces and rotational axes.

Table 1: Atmospheric parameters

Symbol	Value	Unit	Description
P_0	101325	Pa	Pressure at zero altitude (base pressure)
T_0	288.15	K	temperature at zero altitude
g	9.80665	m/s^2	acceleration due to gravity
L	$-6.5*10^{-3}$	K/m	lapse rate
R	287.053	J / (kg K)	gas constant for air
Rh	0 %	dimensionless	relative humidity
M	0.0289644	kg/mol	Molar mass of dry air
R_0	8.31447	J/(mol•K)	Universal gas constant

The theorem stated that the air pressure above the wing is less than the air pressure below the wing. In addition, the amount of AP depends on the intensity of air molecules and moisture content in the space. A low AP will occur when the air in the equatorial region heated up and becomes lighter. While, high pressure arises as the cold air in the equatorial region sinks (Steffen and Box, 2001). Previous studies unveil the use of AP to compute the relationship between altitude and pressure. Most of the parameters in Table 1 were used in hydrostatic equilibrium model, hypsometry model, and a model using a constant lapse rate. In 1830, Löff invented the theory of hydrostatic equilibrium shown in (Equation 1). The equation was used to examine the relationship between AP and altitude. To apply Löff equation, change in AP in relation to a small change in altitude must oppose gravitational force of the surrounding air (Portland State Aerospace Society 2004).

$$\frac{\delta P}{\delta Z} = -\rho g$$

Equation 1

Where p, z, ρ, and g are pressure, altitude, air density, and acceleration due to gravity in that order. The negative sign in the equation implies that AP decreases with altitude. One great drawback in the use of Löff equation is that it is not easy to measure density of gas in meteorological application. Hence, the use of hypsometry equation, which was derived from the hydrostatic equation and the ideal gas law.

Hypsometry model is shown in Equation 2, the equation was developed by Langebein in 1947 to analyze the slope of terrain (Pradeep and Vinaya, 2016, Rivera et al., 2011 and Singh et al., 2008). The model has also been used to explore the relationship between AP and altitude with the assumption that temperature and gravity are constants (Portland State Aerospace Society 2004).

$$Z = -\frac{RT}{g} Log[\frac{P}{P_0}]$$

Equation 2

Where R is the air gas constant and T is the temperature. The negative side of this model is based on the assumption of zero lapse rate. Thus, it should not be encouraged to be used for altitude determination unless an acceptable constant temperature is used (Portland State Aerospace Society, 2004). Conversely, hydrostatic model, in (Equation 3) can be used to show the relationship between AP and altitude using a constant lapse rate that considers temperature as a linear variable, which changes as altitude changes.

$$Z = \frac{T_0}{L}((\frac{P}{P_0})^{-LR/g} - 1)$$

Equation 3

The value of L at near ground surface is a negative number (Table 1). Although, many existing models can be used to show the relationships between pressure and altitude. However, effective use of these models hangs on the ease of obtaining atmospheric parameters.

2.3 Analytical Assessment of the Impact of AP on DEM

2.3.1 Study location

The study was carried out in the golf course area of the Universiti Putra Malaysia. The golf course is in the southern part of the campus. It is about 1km away from the university's main sport centre. The place is at longitude 101^0 43′ 19.08″ E and 101^0 43′ 32.59″ E, and latitude 2^0 59′ 12.87″ N and 2^0 59′ 06.66″ N. The site was chosen due to its nature that suitable for assessing distinct elevations. Besides, the safety of taking-off and landing without obstructing the commercial space route is considered.

2.3.2 Data acquisitions

In this study, data were collected using a fixed-wing UAV platform on-board canon digital camera. The camera has a resolution of 4000 x 3000 megapixels, which was pre-set to take photos every 3 seconds. The camera focal length is fixed, while the skew and radial lens distortion can vary based on the degree

of stability of the camera interior orientation parameters (Fraser, 2012). The UAV is a lightweight unit of about 1.5 kg with a total payload of 600g. It can hover for about 45 minutes in space to cover 250 hectares per flight. The UAV can collect data within the range of 100-700 metres altitude at a wind speed below 25 knots. The inertial measurement unit integrated with the system enables the measurement of altitude, acceleration, magnetic direction, and angular orientation of the aircraft. A barometric pressure sensor in an autopilot system computed AP at different altitudes, which enhances the GPS receivers return altitude data. Before collecting UAVs data, a real time kinematic differential global positioning system was used to establish thirty-nine ground control points (GCPs) within the study area. The GCPs were later used for image processing and quality assessment of UAV DEMs. An unmanned aerial vehicle mapping system involves the collection of reference data, pre-flight planning, real data collection, and exporting of raw photos. Figure 2 (a-b) shows the main data collection steps. Polygon representing the flight lines was drawn using mission planner software, Google map, and some selected GCPs along the boundary lines. A good flight plan enhances image orientation and good photogrammetric products (Komarek et al., 2016 and Martin et al., 2016). In addition, other parameters selected to achieve the study's objective are flying altitudes (100m, 150m, 200m, 250m, 350m, 400m, and 500m), 80% overlap, and 60% side-lap. In the end, seven mission plans were produced for the flight trajectory. The UAVs was launched soon after the pre-flight test. The mission lasted for about 3hrs 30 minutes and then downloaded the recorded photos and log files for data processing.

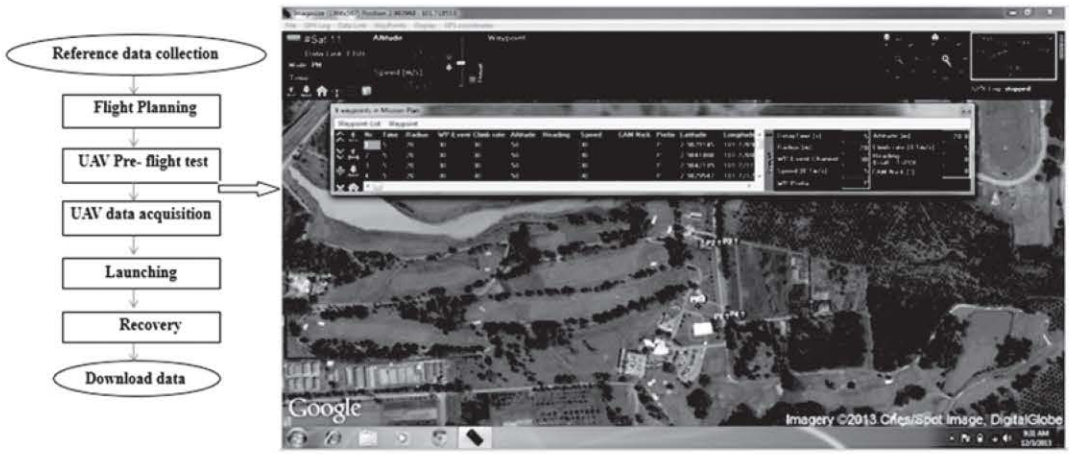

(a) (b)

Figure 2: (a) Image acquisition workflow; (b) flight planning pane

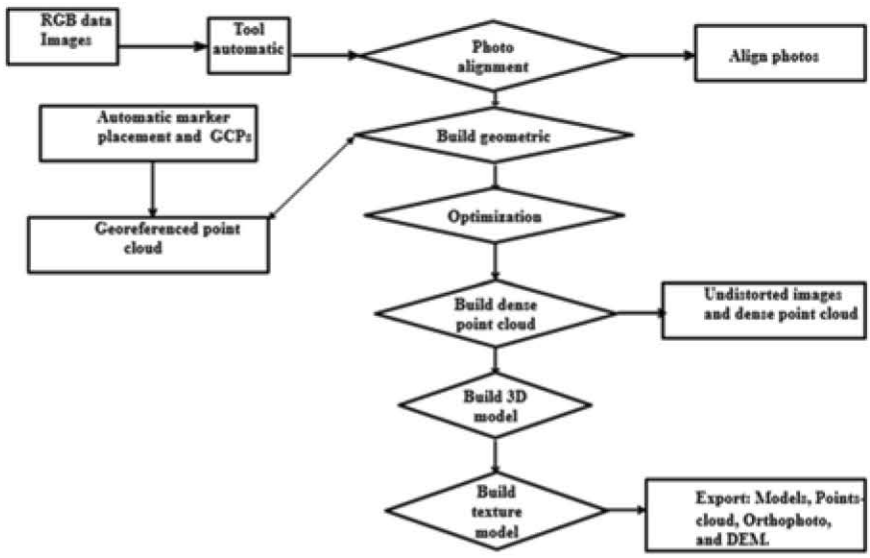

Figure 3: Image processing workflow

2.3.3 Data processing

The size of drone data is large and needs high memory and hardware computer system. The photos were uploaded, in batches. UAV processing step begins with photo alignment (Figure 3). Prior to photo alignment, some extra and low quality photos were removed to prevent extreme details that might affect the quality of the resulting models. Inner orientation allows restitution of geometry integrity of the photos. The photos were orthorectified using a guided marker method. Guided marker approach is a quicker way of relating the position of points on the photos to their analogous point on the ground surface. Guided marker placement is another method of optimizing position and orientation of the camera. However, there is a need to build point geometry to define projection for the photos. Otherwise, the model will lack basic details for markers placement. At this stage, ten out of thirty-nine GCPs were used to enhance the quality of exterior orientation parameters of the photos.

Accuracy and speed of the aligned photos were controlled by three alignment parameters setting "low, medium, and high" in the toolbox. The low setting is faster and suitable for coarse estimation of camera positions. While, the high option used in this study offers accurate camera positions, but takes a longer time. PhotoScan uses estimated camera positions to generate depth information for dense point cloud that forms the basis for DEM generation (Thoeni et al., 2014 and Fraser, 2012). Like sparse point cloud, higher quality setting mode provides accurate DEMs. The in-built algorithm filter removes outliers that might affect the quality of the resulting model. Other extreme outliers were removed manually. Mesh and texture models may be ignored if a 3-D polygonal model is not required. The remaining twenty-nine GCPs were used as check points for validating the quality of the resulting models. The entire processing time took about 42 hrs.

2.3.4 Impact of atmospheric pressure on DEM

In this section, the effect of AP on the quality of DEMs was measured using Equation 4 and Equation 5. To the best of our knowledge, this is the first time that the impact of AP on the DEM derived from UAV system would be assessed using the proposed models below.

$$p = k/h \qquad \text{Equation 4}$$

$$k = h(\rho/A) \qquad \text{Equation 5}$$

Where h, ρ, p and A are altitude, point density, impact and coverage area in that order. The values of h, ρ, and A can be obtained from the PhotoScan processing report. Value of "k" at different altitudes was computed using Equation (5). While, the impact "p" was computed by substituting "k" in the Equation 4 and got 0.072m, 0.048m, 0.014m, 0.01m, 0.004m, 0.003m, and 0.002m for the DEMs at 100m, 150m, 200m, 250m, 350m, 400m, and 500m altitudes in that order. The results were validated using the remaining GCPs and got RMSE of 0.03m, 0.05m, 0.07m, 0.1m, 0.13m, 0.14m, and 0.16m for the DEMs acquired at the altitudes stated above, respectively.

3. Results and Discussion

This section discusses the results of the findings. Figure 4a and 4b shows three-dimensional representations of the study area. Colour ramp was used to classify the relief of the study area (Harwin and Lucieer, 2012). As can be seen in the figure, colour blue and red denote minimum and maximum elevations respectively. Likewise, Table 2 above presents a summary of the findings. As can be seen in the table, the observed and validated results are highly correlated. Similarly, at the 100m altitude, resolution and point density of the DEM are higher than resolution and point density of the DEMs produced at altitudes above 100m. Concisely, altitude is inversely proportional to the point density per square meter and, directly proportional to the coverage area of the models.

Amidst all the DEMs represented by the histogram shown in Figure 5 above, the DEM acquired at 100m altitude produced highest-level of accuracy even with the largest impact of the AP. As can be seen in the figure, at the 100m altitude, the numerical values of the impact of AP and the DEMs RMSE are accidentally equal. At this altitude, the DEM accuracy is better than the accuracy of the DEMs acquired at altitudes higher than 150m. Accuracy of the DEM at 500m altitude is lesser than accuracy of the remaining DEMs even at a nearly zero impact of the AP. Briefly, the foregoing reveals that the influence of AP decreases as altitude increases and contrarily. Whereas, accuracy of the resulting digital elevation model increases as altitude decreases.

Multiple regression analysis results are shown in Table 3 above. The table also reports information about the relationships between impact of AP and altitude, and RMSE. Multiple R-value in the table shows how well the data clusters around the regression line. The closer this value is to 1, the more linear the data.

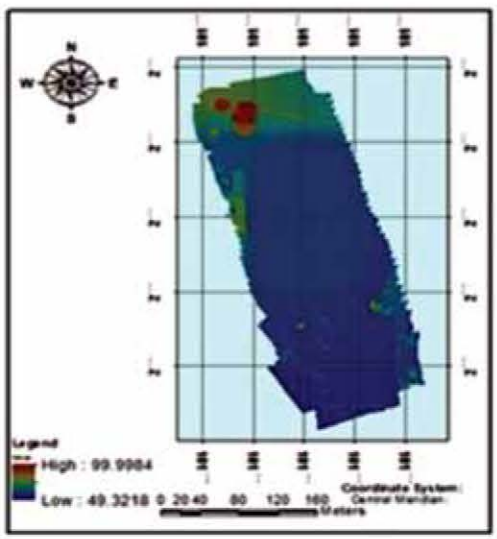

(a)- 150 m

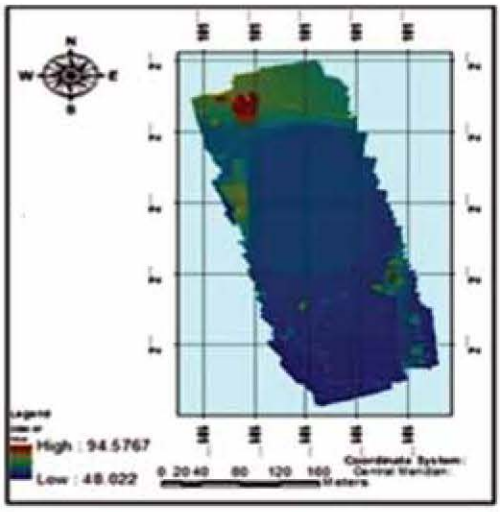

(b)- 250 m

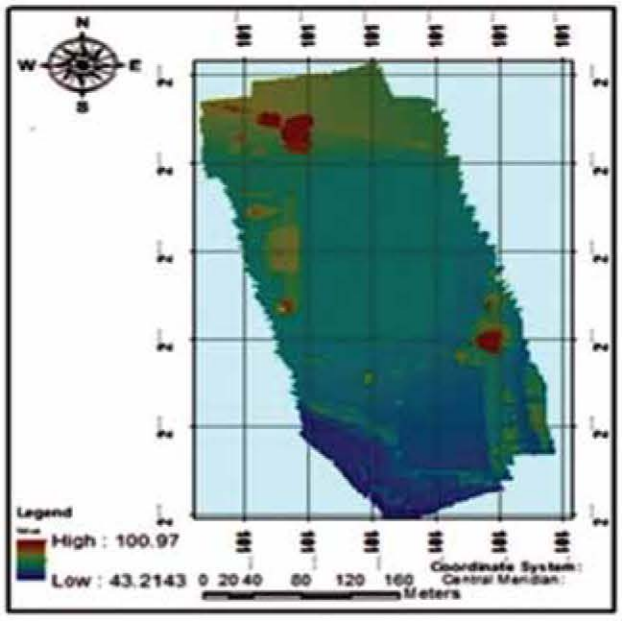

(c)- 350 m

Figure 4a: Reconstructed digital elevation model generated at an altitude of 150m, 250m, and 350m.

Table 2: Image processing report and analysis

		Reconstructed Digital Elevation Model					
Flying altitude (m)	100	150	200	250	350	400	500
Coverage Area (sq.km)	0.07	0.12	1.22	1.28	1.72	1.76	1.81
Resolution (cm/pix)	4.47	6.2	10.52	12.5	18.4	19.98	22.71
Point Density(point/sqm)	365.1	271.3	247.3	145.1	29.5	17.00	6.50
p (m) impact	0.072	0.05	0.014	0.01	0.004	0.003	0.002
RMSE (m) validated	0.03	0.05	0.07	0.1	0.13	0.14	0.16

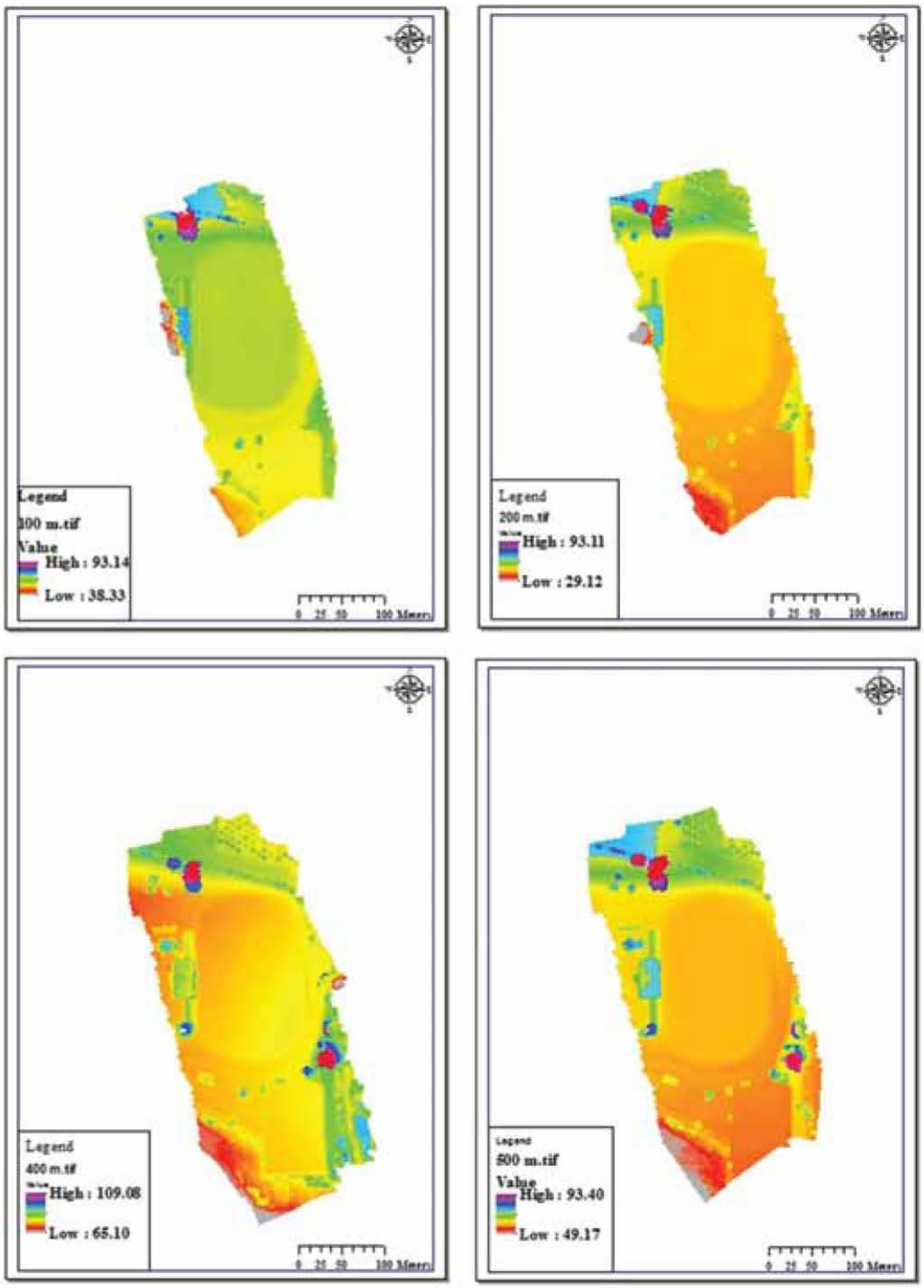

Figure 4b: Reconstructed digital elevation model generated at 100m, 200m, 400m, and 500m respectively.

Similarly, 0.867 R square reported in the table is an indication of goodness-of-fit. The closer this value is to 1 the better is the regression line fitted the data. Reliability of the results can also be judged using Significance F value, which is 0.018 in this study. Hypothetically, a model is considered reliable if the value of Significance F is less than 0.05. Graphical plots of Table 3 provide a point-by-point visual appraisal of the models. The RMSE and the impact of AP were shown in Figure 6 (a) and (b) respectively. As can be seen in the figure, the residuals are found close to the zero lines. This indicates the smallness of the residual values and in essence shows that the curve was precisely fitted to the data points. Indeed, the pattern of the graphs exhibit good quality of a simple linear regression models because they are normally distributed around the horizontal axis.

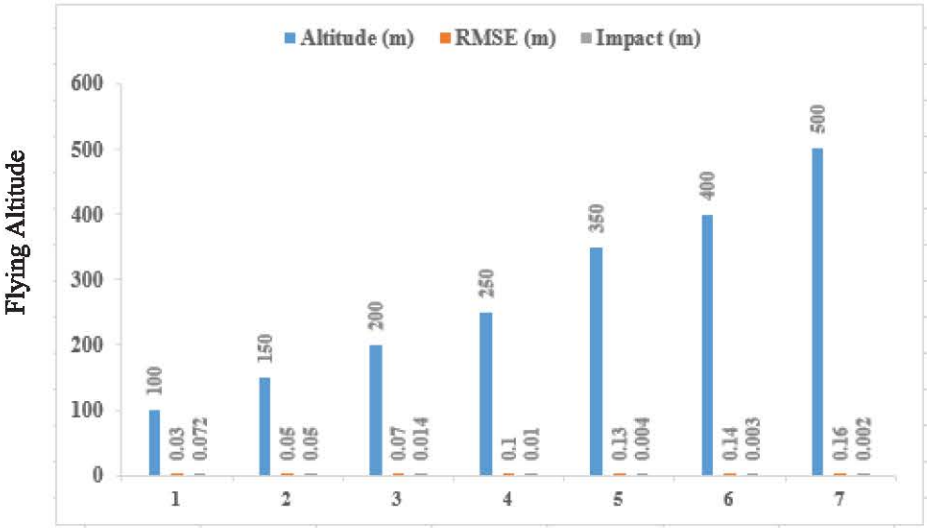

Figure 5: Quality relationships chart.

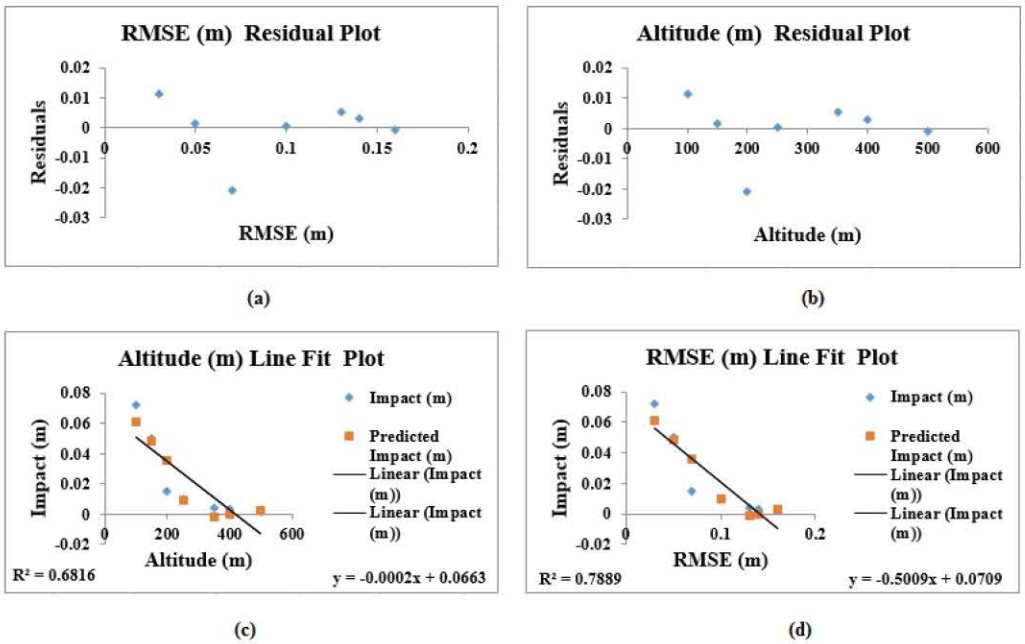

Figure 6: Residual plots.

Similarly, Figure 6 (c) and (d) shows negative linear relationships between the impact of AP and flight altitude, and RMSE. The negative patterns show that AP impact and altitude move in the opposite direction (that is, as the altitude increases AP impact decreases). This negative correlation shows a strong relationship, especially when R square is close to 1. Therefore, the numerical values of R square for the graphs clearly indicate that the regression models fit the data.

4. Conclusions

Previous studies show the relationships between atmospheric pressure (AP) and altitude using equations that depend on atmospheric parameters. However, the current study explores the impact of AP on the quality of DEMs produced by UAV system using our proposed equations. The study covers both manned and unmanned aircraft. Although, UAV remote sensing platform offers many benefits. Yet, it is not suitable for wooded terrain and requires high computational tasking particularly when used for large area mapping. The paper discusses two important issues in stages. The first stage reviews interaction of external forces with aircraft in relation to AP and altitude. While, the second stage examines the effect of AP on the quality of UAV-based DEMs using proposed models and unveiled that the impact is insignificant.

Table 3: Multiple regression analysis results

SUMMARY OUTPUT

Regression Statistics	
Multiple R	0.931362611
R Square	0.867436313
Adjusted R Square	0.801154469
Standard Error	0.012295119
Observations	7

ANOVA

	df	SS	MS	F	Significance F
Regression	2	0.003956749	0.001978374	13.0870879	0.017573131
Residual	4	0.00060468	0.00015117		
Total	6	0.004561429			

	Coefficients	Standard error	t start	P-value	Lower 95%	Upper 95%	Lower 95%	Upper 95%
Intercept	0.071862205	0.011018715	6.521831599	0.002854264	0.041269347	0.102455063	0.041269347	0.102455063
Altitude	0.000307218	0.000199589	1.539250639	0.198577932	-0.000246931	0.000861366	-0.000246931	0.000861366
RMSE	-1.391338583	0.58752976	-2.368115928	0.076978779	-3.022582709	0.239905543	-3.022582709	0.239905543

RESIDUAL OUTPUT

Observation	Predicted Altitude	Residuals	Standard Residuals
1	0.060843832	0.011156168	1.111291374
2	0.048377953	0.001622047	0.161575831
3	0.035912073	-0.020912073	-2.083099405
4	0.009532808	0.000467192	0.046538022
5	-0.001485564	0.005485564	0.54642959
6	-3.80577E-05	0.003038058	0.302627871
7	0.002856955	-0.000856955	-0.085363283

Further analysis was carried out using linear multiple regression in which it was revealed that AP decreases as altitude increases and contrarily. Based on the results, the impact of AP can be ignored amidst of other external forces that can influence the quality of UAV products. Ignoring the AP impact does not mean that the DEMs are error-free.

Future work will be required to explore the impact of other factors on the DEM produced by the UAV system. That research will help to identify factors with higher impact value before subjecting the DEM to a standard accuracy enhancement packaging that will enhance its quality to meet up with precision applications.

Acknowledgments

The authors appreciate the efforts of the staff and management of the Universiti Putra Malaysia for funding the UAV project. We also thank Geospatial Information Science Research Centre (GISRC) unit and JUPEM for their great input to achieve the goal of this study.

References

AGARD, 1980, Special Course on Missile Aerodynamics. Vol. 53. (Rhode-St-Genise, Belgium).

Aguilar, M. A., Aguilar, F. J., Antonio, F., Fernández, I., Saldaña, M. M., García Lorca, A. M., Negreiros, J. G., Viciana, A. and González, E., 2011, Geometric Processing of GeoEye-1 Satellite Imagery for Coastal Mapping Applications. *In International Conference on Innovative Methods in Product Design June 15th – 17th, 2011*, Venice, Italy ADM – INGEGRAF, 9. Venica. https://w3.ual.es/ Proyectos/ GEOEYE1WV2/ index_archivos/IMProVe2011 _MAAT_et_al_2011.pdf.

Ajibola, I. I. and Mansor, S., 2013, UAV-Based Imaging for Environmental Sustainability - Flash Floods Control Perspective UAV-Based Imaging for Environmental Sustainability - Flash Floods Control Perspective. *In FIG Conference, 1–15.* Abuja.www.fig.net/pub/fig2013/ papers/ts01c/ TS01C_ ajibola_ shattri_6548.pdf.

Ajibola, I., Mansor, S., Pradhan, B., and Helmi, S., 2015, UAV- Based Imaging – Digital Elevation Model Extraction. *In FIG Working Week 2015 from the Wisdom of the Ages to the Challenges of the Modern World*, 17–21. Sofia.

Akbari, A., Noram, I. R. and Ngien, S., 2016, Application of Public Domain Satellite-Based DEMs in Natural Hazard Modelling. *International Journal of Environmental Science and Development,* Vol. 7(2): 140-44. doi:10.7763/IJESD.2016.V7.756

Paul, A., and Ferl, R. J., 2006, The Biology of Low Atmospheric Pressure-Implications for Exploration Mission Design and Advanced Life Support. *Gravitational and Space Biology*, Vol. 19(2), 3-18.

Austin, R., 2010, *Unmanned Aircraft Systems UAVS Design, Development and Deployment.* Edited by Allan Seabridge and Roy Langton Lan Moir. 1st edition (*John Wiley and Sons, Ltd*).

Boschetti, P., Elsa, C., Andrea, A. and Angela, A., 2010, Stability and Performance of a Light Unmanned Airplane in Ground Effect. *48th AIAA Aerospace Sciences Meeting Including the New Horizons Forum and Aerospace Exposition.* doi:10.2514/6.2010-293.

Cheng, P. and Chaapel, C., 2014, Mapping Large Areas Satellite Imageries with Limited Ground Control. *GEOInformatics*, 34-39, https://pdfs.semanticscholar.org/a976/191acbf502d02524f034925ac9ee39fa3ece.pdf.

Edwards, A., 1988, Volume II. Flying Qualities Phase. Chapter 8: Dynamics. *USAF Test Pilot School*. www.dtic.mil/get-tr-doc/pdf?AD=ADA-319975.

Ehernberger, L. J., 1992, Stratospheric Turbulence Measurements and Models for Aerospace Plane Design. California.https://ntrs.nasa.gov/archive-/nasa/casi.ntrs.nasa.gov/19930004100.pdf.

Forkuor, G. and Maathuis, B., 2012, Comparison of SRTM and ASTER Derived Digital Elevation Model over Two Regions in Ghana - Implifications for Hydrogical and Environmental Modelling. *InTech*, Vol. 9, 219-240. doi:10.5772/1522.

Fraser, C. S., 2012, Automatic Camera Calibration in Close-Range Photogrammetry. *ASPRS 2012 Annual Conference*, 1–9. Sacramento, California. http://www.close-range.com/docs/AUTOMATIC_CAMERA_CALIBRATION_IN_CLOSE_RANGE_PHOTOGRAMMETRY_Fraser.pdf.

Harwin, S. and Arko, L., 2012, An Accuracy Assessment of Georeferenced Point Clouds Produced Via Multi-View Stereo Techniques Applied to Imagery Acquired Via Unmanned Aerial Vehicle. *ISPRS - International Archives of the Photogrammetry, Remote Sensing and Spatial Information Sciences*. 475-480. doi:10.5194/isprsarchives-XXXIX-B7-475-2012.

Hull, D. G., 2007, *Fundamentals of Airplane Flight Mechanics*. Springer-Verlag Berlin Heidelberg. doi:10.1007/978-3-540-46573-7.

Kalra, A., Anand, P. and Singh, S., 2014, Flight Simulation Using Graphical User Interface. *Advances in Aerospace Science and Applications*, Vol. 4(1): 85–90. http/:www.ripublication.com/aasa.htm.

Khairul, N. T. and Anuar, A., 2013, An Evaluation on Fixed Wing and Multi-Rotor UAV Images Using Photogrammetric Image Processing. *World Academmy of Science, Engineering and Technology*. Vol. 73 (1), 348–52. http://www.waset.org/publications/11861.

Komarek, J., Kumhalova J. and Kroulik, M., 2016, Surface Modelling Based on Unmanned Aerial Vehicle Photogrammetry and Its Accuracy Assessment. *Engineering for Rural Development*, 888–892. http://tf.llu.lv/conference/proceedings2016/ Papers/N168.

Li, Z., Yu, Y., Yabing, J. and Shu, G. Z., 2015, The Design and Testing of a LiDAR Platform for a UAV for Heritage Mapping. *International Archives of the Photogrammetry, Remote Sensing and Spatial Information Sciences*, Vol. XL-1/W4, 17–24. doi:10.5194/isprsarchives-XL-1-W4-17-2015.

Martin, P. G., Kwong, S., Smith, N. T., Yamashiki, Y., Payton, O. D., Russell-Pavier, F. S., Fardoulis, J. S., Richards, D. A. and Scott, T. B., 2016, 3D Unmanned Aerial Vehicle Radiation Mapping for Assessing Contaminant Distribution and Mobility. *International Journal of Applied Earth Observation and Geoinformation*, Vol. 52, 12-19. http://dx.doi.org/10.1016/j.jag.2016.05.007.

Marzocca, P., 2013, AE 430 - Stability and Control of Aerospace Vehicles. http://people.clarkson.edu/~pmarzocc/AE430/AE-430-7.pdf

Mercuri, P. A., Engel, B. A. and Johannsen, C. J., 2006, Evaluation and Accuracy Assessment of High-Resolution IFSAR DEMs in Low-Relief Areas. *International Journal of Remote Sensing*, Vol. 27(13), 2767–2786. Doi: 10.1080/01431160500491716.

Moore, I. D., Grayson, R. B. and Ladson, A. R., 1991, Digital Terrain Modelling: A Review of Hydrological, Geomorphological, and Biological Applications. *Hydrological Processes,* Vol. 5(1), 3–30. Doi: 10.1002/ hyp. 3360050103.

Nex, F., 2016, The Use of Uavs for Earth Observation. https://webapps.itc.utwente.nl/librarywww/papers_2015/pres/nex_use_ppt.pdf.

Padfield, G. D. and Lawrence, B., 2003, The Birth of Flight Control: An Engineering Analysis of the Wright Brothers' Flyer. *The Aeronautical Journal*, 697-718. http://pcwww.liv.ac.uk/ew-eb/fst/ publications/2854.pdf.

Papasaika-Hanusch, C., 2012, Fusion of Digital Elevation Models. Institute of Geodesy and Photogrammetry ETH ZURICH CH-8093. www.igp-data.ethz.ch/berichte/Blaue_Berichte_-PDF/109.pdf (Accessed August 17, 2018).

Portland State Aerospace Society, 2004, A Quick Derivation Relating Altitude to Air Pressure. 1-4. http://psas.pdx.edu/RocketScience/PressureAltitude_Derived.pdf.

Pradeep, P. and Vinaya, M. S., 2016, GIS and Hypsometry Based Analysis on the Evolution of Sub Basins of Ponnaiyar River, Krishnagiri District, Tamil Nadu. *International Journal for Innovative Research in Science & Technology*, Vol. 2(10), 1–8.

Rivera, A., Fiona, C., Camilo, R. and Clauidio, B., 2011, Hypsometry. *Encyclopedia of Snow Ice and Glaciers*, 551–554. doi:10.1029/2006WR-005022.Stenborg.

Sciavicco, L. and Bruno, S., 2000, *Modelling and Control of Robot Manipulators*. 2nd ed. London: Springer-verlag. Doi: 10.1007/978-1-4471-0449-0.

Singh, O., Arjamadutta, S. and Milap, C. S., 2008, Hypsometric Integral Estimation Methods and Its Relevance on Erosion Status of North-western Lesser Himalayan Watersheds. *Water Resources Management*, Vol. 22(11), 1545–1560. Doi: 10.1007/s11269-008-9242-z.

Steffen, K. and Jason, B., 2001, Surface Climatology of the Greenland Ice Sheet: Greenland Climate Network 1995-1999. *Journal of Geophysical Research*, Vol. 106(24), 33951-33964, Doi: https://doi.org/10.1029/2001JD-900161

Talay, T. A., 1975, Introduction to the Aerodynamics of Flight [NASA SP-367]. Scientific and Technical Information Office National Aeronautics and Space Administration. Washington, D.C.

Thoeni, K., Giacomini, A., Murtagh, R. and Kniest, E., 2014, A Comparison of Multi-View 3D Reconstruction of a Rock Wall Using Several Cameras and a Laser Scanner. *International Archives of the Photogrammetry, Remote Sensing and Spatial Information Sciences*. Vol. 40(5), 573-80. Doi: 10.5194/isprsarchives-XL-5-573-2014.

Thomas, J., Joseph, S., Thrivikramji, K. P. and Arunkumar, K. S., 2014, Sensitivity of Digital Elevation Models: The Scenario from Two Tropical Mountain River Basins of the Western Ghats, India. *Geoscience Frontiers*, Vol. 5(6). 893-909. doi:10.1016/j.gsf.2013.12.008.

Walker, J. P. and Garry, R. W., 1999, On the Effect of Digital Elevation Model Accuracy on Hydrology and Geomorphology. Water Resources Research, Vol. 35(7), 2259–2268. Doi: 10.1029/1999WR900034.

Wechsler, S., 2006, Uncertainties Associated with Digital Elevation Models for Hydrologic Applications: A Review. Hydrology and Earth System Sciences Discussions, Vol. 3, 2343-2384. Doi: 10.5194/hess-11-1481-2007.